Coastal Engineering 41 (2000) 295–316
COASTAL ENGINEERING
www.elsevier.com/locate/coastaleng

Tide, turbulence and suspended sediment modelling in the eastern English Channel

Georges Chapalain *, Laurent Thais

Laboratoire de Sédimentologie et Géodynamique, UMR-CNRS 8577, Bâtiment SN5, Université des Sciences et Technologies de Lille, Villeneuve d'Ascq F-59655, France

Abstract

The present paper is concerned with modelling fluid and suspended sediment dynamics in a tide-dominated environment. The procedure consists of a one-dimensional vertical model driven by an oscillatory horizontal pressure gradient derived from a two-dimensional vertically integrated tidal model. The vertical model includes two linearised momentum equations for the horizontal velocity components and a series of advection–diffusion equations for concentrations of suspended sediment of specific size. Turbulence generated at the seabed is computed with the aid of a two-equation closure describing the time–space evolution of the turbulent kinetic energy k and of the dissipation rate of the turbulent kinetic energy ε (standard $k-\varepsilon$ model). A mixed type bottom boundary condition for the sediment concentration equations is adopted to take into account downward fluxes at times of decelerating flow and slack waters.

The model is applied to the eastern part of the English Channel. The tidal currents, turbulent kinetic energy and the total suspended sediment load predicted by the model are compared with field data collected in two sites. The vertical structure of these flow properties is fairly well predicted by the present model. Better results are found at the measuring point located farther from the coastline where advective terms can be reasonably neglected. © 2000 Elsevier Science B.V. All rights reserved.

Keywords: Measurements; Numerical modelling; Suspended sediment; Tidal bottom boundary layer; Turbulence

1. Introduction

In the eastern English Channel (Fig. 1), tidal currents are strong and interact with the bottom sediment yielding intense sediment transport. Suspended sediment affects the

* Corresponding author. Fax: +33-3-2043-4910.
E-mail address: georges.chapalain@univ-lille1.fr (G. Chapalain).

PII: S0378-3839(00)00038-7

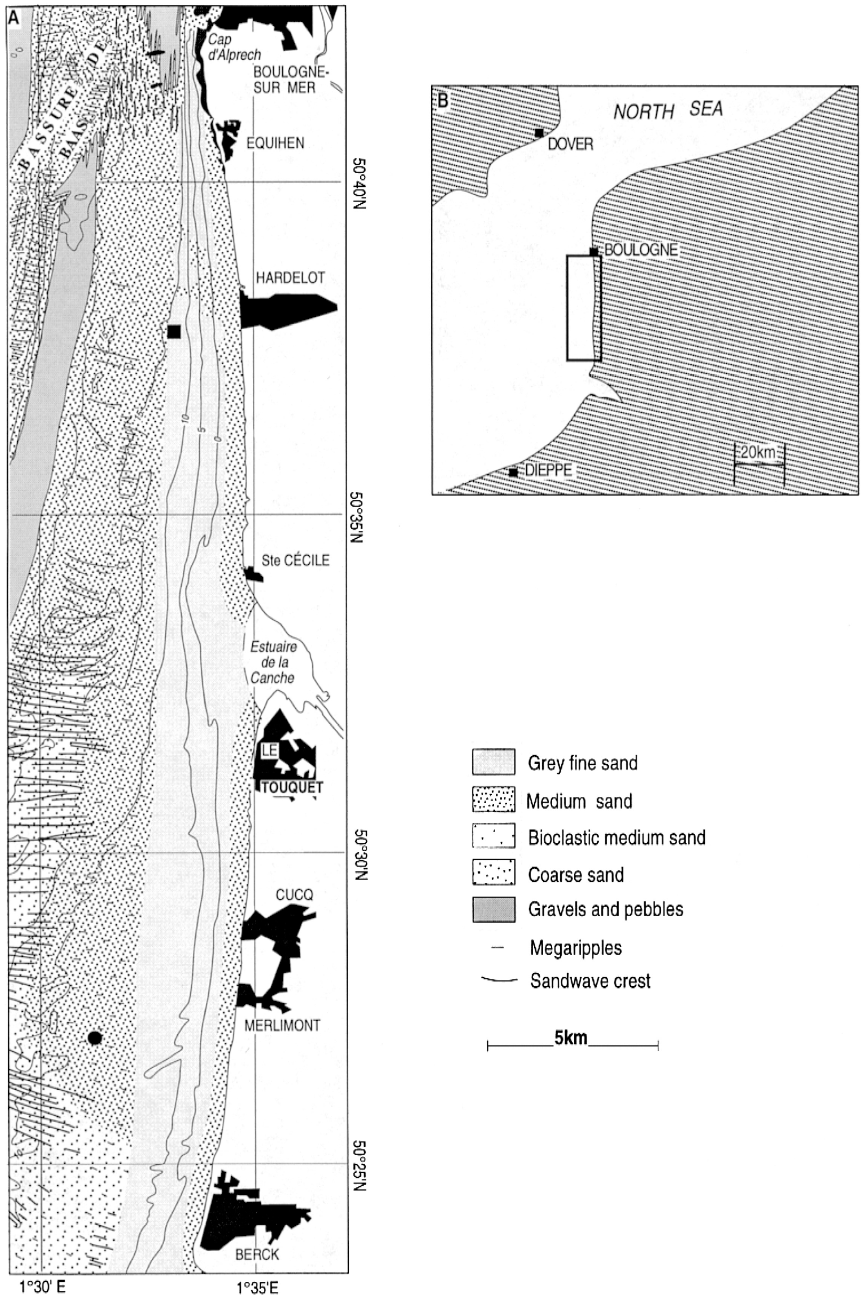

Fig. 1. Study area, (A) bathymetry and surficial sediment in the vicinity of the measurement sites (■ Hardelot site, ● Merlimont site) (from Augris et al., 1987), (B) computational domain of the two-dimensional vertically integrated model.

marine environment in a variety of ways (e.g. evolution of bottom topography, water clarity, transport of contaminants attached to fine particles, development of stratigraphy); hence, the ability to predict its behaviour is of great scientific and practical importance.

The vertical structure of current and suspended sediment concentration depends on the distribution of turbulence in the bottom boundary layer. In order to model the distribution of these properties describing the sediment-laden flow, the generation of turbulence near the seabed, together with the dissipation, diffusion, and transport of turbulent energy, as well as the entrainment and deposition of particles at the seabed, must be represented accurately.

As an alternative to fully three-dimensional tidal models, here we propose to use a one-dimensional vertical model forced by horizontal pressure gradients computed with the aid of a two-dimensional vertically integrated tidal model (Hess, 1986). This procedure is computationally more cost-effective than the fully three-dimensional approach in which the vertical mesh has to remain relatively coarse for obvious computational constraints. The improvement in the vertical description of the flow is offset by the loss of the advective terms in the field equations. We shall examine in this paper whether we are able to predict the tidal flow in spite of this simplification. Details about the two-dimensional tidal model used to provide the pressure gradients can be found in Hess (1986) and will not be repeated here. The focus of the paper will be on the description of the one-dimensional vertical model (Sections 2 and 3).

A key issue in the modelling approach was the choice of the turbulence closure to predict vertical mixing. Among many closures available (see e.g. Rodi, 1980, 1981, 1987; ASCE Task Committee on Turbulence Models in Hydraulic Computations, 1988a,b; Davies et al., 1995; Baumert et al., 2000), we selected the standard two-equation $k-\varepsilon$ model. Our choice was motivated by a recent analysis of turbulent kinetic energy time series from data collected in the English Channel and in the Elbe estuary (Baumert et al., 2000; Chapalain and Thais, 2000).

The present model is used to simulate the tidal flow in the eastern part of the English Channel. The model predictions are compared with observations collected at the two measuring points of a recent field experiment involving measurements in the inner and outer bottom boundary layer. The measurement sites, experimental arrangement, and data reduction procedures are briefly described in Section 4. Comparisons with model predictions are given in Section 5 and we summarise our main findings in Section 6.

2. Model formulation

2.1. Assumptions

The model to be presented is for horizontally uniform, oscillatory rough turbulent boundary layer flow. This is a reasonable approximation for tidally driven flows. Depth variations associated with the tidal wave are assumed to be negligible.

The sedimentary particle assemblage is treated as a number of components of different grain sizes. Individual particles are assumed to be spherical, non-cohesive and made of quartz with density ρ_s equal to 2650 kg m^{-3}. Additional constraints must be placed upon the particle size in order to ensure that the fluid–sediment mixture retains the Newtonian behaviour of a clear fluid. It is therefore assumed that the smallest length scale of the turbulence is large in comparison with the largest particle size (Barenblatt, 1953). For a typical friction velocity $u^* \sim 10^{-2}$ m s^{-1} in the eastern part of the English Channel, the dissipation rate is of order $\varepsilon \sim 2 \times 10^{-6}$ m^2 s^{-3}, which corresponds to a Kolmogorov microscale of turbulence $l_\kappa \sim 800$ μm. This can be safely considered as large compared with the largest particles likely to move in suspension under average tidal conditions.

It is also supposed that the particle concentration is high enough to represent a continuum, but low enough to neglect particle interactions (< 8 g l^{-1}; Lumley, 1978). It is further assumed that the inertia of the particles is small (Soo, 1967; Lumley, 1978), so that except for a systematic constant settling velocity, the particles follow the mean flow.

The effects of stratification due to suspended sediment are neglected on the basis of the criterion of Soulsby and Wainwright (1987). Typical conditions encountered in the study area fall in regime I where stratification is insignificant (see Fig. 2 in Soulsby and Wainwright, 1987). Thermohaline stratification is also neglected.

2.2. Mean equations

With these simplifications, the linearised, Reynolds-averaged governing equations for the tidal flow in a right-handed Cartesian coordinate system with x eastward, y northward, and z positive upward from the seabed are given by:

$$\frac{\partial\langle u\rangle}{\partial t} = -\frac{1}{\rho}\frac{\partial\langle p\rangle}{\partial x} + f\langle v\rangle - \frac{\partial\langle u'w'\rangle}{\partial z}, \tag{1}$$

$$\frac{\partial\langle v\rangle}{\partial t} = -\frac{1}{\rho}\frac{\partial\langle p\rangle}{\partial y} - f\langle u\rangle - \frac{\partial\langle v'w'\rangle}{\partial z}. \tag{2}$$

In the above equations, t is the time, u, v, and w are the x, y, and z velocity components, ρ is the water density, p denotes the pressure, and f is the Coriolis parameter equal to $2\Omega\sin(\varphi)$ with $\Omega = 7.29 \times 10^{-5}$ rad s^{-1} and φ the latitude. The angular brackets represent the Reynolds averaging process and the prime denotes turbulent fluctuations.

The forcing functions in Eqs. (1) and (2) are the components of the horizontal pressure gradient, which can be written in terms of an oscillating sea surface slope as $\nabla\langle p\rangle = \rho g \nabla\zeta$, where ζ is the sea surface elevation and g is the acceleration of gravity.

The equation of conservation of a single class of suspended sediment reads:

$$\frac{\partial\langle c_i\rangle}{\partial t} = w_{si}\frac{\partial\langle c_i\rangle}{\partial z} - \frac{\partial\langle c_i'w'\rangle}{\partial z}. \tag{3}$$

Here c_i denotes the volumetric concentration of suspended sediment in class i, and w_{si} is the corresponding settling velocity. Assuming the fine material remains non-cohesive, we use Stokes' law for particles of diameter $d_i < 63$ μm:

$$w_{si} = \frac{g d_i^2(\rho_s/\rho - 1)}{18\nu_0}, \tag{4}$$

and the empirical relationship for particles of diameter $d_i \geq 63$ μm after Gibbs et al. (1971):

$$w_{si} = \frac{-3\nu_0 + \sqrt{9\nu_0^2 + g d_i^2 (\rho_s/\rho - 1)(\alpha_1 + \beta_1 d_i)}}{\alpha_2 + \beta_2 d_i}, \quad (5)$$

where $\nu_0 = 10^{-6}$ m^2 s^{-1} is the kinematic viscosity of the water and the empirical constants are $(\alpha_1, \alpha_2) = (3.869 \times 10^{-5}$ m, 1.1607×10^{-4} m), and $(\beta_1, \beta_2) = (2.4801 \times 10^{-2}, 7.4405 \times 10^{-2})$.

2.3. Turbulence closure

The cross-correlations between fluctuating quantities in Eqs. (1)–(3) are the vertical fluxes of momentum and suspended sediment by turbulent motion. They are determined on the basis of the eddy viscosity υ_t/diffusivity γ_t concept (Boussinesq, 1877), i.e.,

$$-\langle u' w' \rangle = \upsilon_t \frac{\partial \langle u \rangle}{\partial z}, \quad (6)$$

$$-\langle \upsilon' w' \rangle = \upsilon_t \frac{\partial \langle \upsilon \rangle}{\partial z}, \quad (7)$$

$$-\langle c_i' w' \rangle = \gamma_t \frac{\partial \langle c_i \rangle}{\partial z}. \quad (8)$$

The eddy diffusivity γ_t is assumed proportional to the eddy viscosity υ_t:

$$\gamma_t = \upsilon_t / \sigma, \quad (9)$$

where σ is the Prandtl–Schmidt number.

The eddy viscosity υ_t is related to the turbulent kinetic energy k and the dissipation rate of the turbulent kinetic energy ε by:

$$\upsilon_t = C_\mu \frac{k^2}{\varepsilon}, \quad (10)$$

where C_μ is an empirical constant. The turbulent moments k and ε are obtained by solving the following pair of transport equations:

$$\frac{\partial k}{\partial t} = \frac{\partial}{\partial z}\left(\frac{\upsilon_t \partial k}{\sigma_k \partial z}\right) + \upsilon_t \left[\left(\frac{\partial \langle u \rangle}{\partial z}\right)^2 + \left(\frac{\partial \langle \upsilon \rangle}{\partial z}\right)^2\right] - \varepsilon, \quad (11)$$

$$\frac{\partial \varepsilon}{\partial t} = \frac{\partial}{\partial z}\left(\frac{\upsilon_t \partial \varepsilon}{\sigma_\varepsilon \partial z}\right) + C_1 \upsilon_t \left[\left(\frac{\partial \langle u \rangle}{\partial z}\right)^2 + \left(\frac{\partial \langle \upsilon \rangle}{\partial z}\right)^2\right] \frac{\varepsilon}{k} - C_2 \frac{\varepsilon^2}{k}. \quad (12)$$

The empirical constants appearing in the model described above take the values given in Table 1.

Table 1
Constants in the $\kappa - \varepsilon$ model

σ	C_μ	σ_k	σ_ε	C_1	C_2
1.3	0.09	1.0	1.3	1.44	1.92

2.4. Boundary conditions

The governing set of partial differential equations Eqs. (1)–(3), (11) and (12) is solved subject to boundary conditions at the seabed and the free surface. The bottom limit of integration for the boundary layer is constrained by the level z_0 defined as the height above the seabed at which the fluid velocity is zero. Ripples being often present for movable beds, z_0 will be estimated in terms of ripple height η and ripple length λ using the empirical relationship after Wooding et al. (1973):

$$z_0 = 2\eta\left(\frac{\eta}{\lambda}\right)^{1.4}. \tag{13}$$

Following Yalin (1972, 1985), the ripple height is taken equal to be $\eta = 100\ d_{50}$ and the ripple length equal to $\lambda = 1000\ d_{50}$ where d_{50} is the median diameter of bottom sediment. This implies $z_0 \sim 8\ d_{50}$.

At the seabed $(z = z_0)$, the no-slip condition reads:

$$u = 0,\ \ v = 0. \tag{14}$$

The bottom boundary condition for the turbulent kinetic energy k is derived assuming local equilibrium between production and dissipation:

$$k = \frac{u_*^2}{\sqrt{C_\mu}}, \tag{15}$$

where $u_* = \sqrt{|\vec{\tau}_\mathrm{b}|/\rho}$ is the modulus of the friction velocity based on the total bottom shear stress spatially averaged over one ripple wavelength $\vec{\tau}_\mathrm{b} = (-\rho\langle u'w'\rangle, -\rho\langle v'w'\rangle)_{z=z_0}$.

The existence of a universal logarithmic near-bottom layer in rough turbulent flows allows one to assume that the dissipation rate of the turbulent energy ε is:

$$\varepsilon = \frac{u_*^3}{\kappa z_0}, \tag{16}$$

where κ is the Karman constant $(\kappa = 0.4)$.

The bottom boundary condition for the suspended sediment concentrations c_i specifies the net mass flux through the water–sediment interface. This flux is the difference between downward advection due to settling of the particles, or deposition rate D_i and upward entrainment of sediment from the seabed E_i:

$$w_{\mathrm{s}i}\langle c_i\rangle + \gamma_\mathrm{t}\frac{\partial\langle c_i\rangle}{\partial z} = D_i - E_i. \tag{17}$$

In considering the unsteadiness of the tidal flow, this approach is adopted instead of prescribing an instantaneous near-bed suspended sediment concentration. A flux condition is expected to yield physically more sensible results at times of decelerating flow and slack waters by taking into account the pre-existing suspended sediment.

The deposition rate D_i is made proportional to the near-bed suspended sediment concentration with the proportionality factor equal to the settling velocity w_{si} (Eqs. 4 and 5), i.e.,

$$D_i = w_{si} \langle c_i \rangle. \tag{18}$$

This formula is valid for particles of sufficient diameter and density that their settling dominates diffusion near the sediment–water interface (Lick, 1982; Lavelle et al., 1984). This is the case in the present study dealing with medium to coarse silts and sands.

The method used here to specify the entrainment rate E_i follows Celik and Rodi (1984a, 1985, 1988, 1991) and van Rijn (1986). It is based on the physical hypothesis that the flow always entrains as much sediment from the seabed as it can with the energy available. This implies that, for a situation with a loose bed of unlimited sediment material supply, the entrainment always occurs at its maximum rate. This entrainment rate of sediment of class i under full capacity equilibrium situation (i.e., zero net flux across the bottom corresponding to a balance between deposition and entrainment) is:

$$E_i = w_{si} \langle c_{ai} \rangle. \tag{19}$$

The maximum equilibrium near-bed suspended sediment concentration $\langle c_{ai} \rangle$ in Eq. (19) is given by the semi-empirical expression of Smith and McLean (1977):

$$\langle c_{ai} \rangle = f_i c_b \left(\frac{\gamma_0 s_i}{1 + \gamma_0 s_i} \right), \tag{20}$$

where f_i is the fractional percentage of bottom sediment in size class i provided by a grain size analysis, c_b is the total volume concentration of sediment in the settled bed (1 − porosity) here taken as 0.65, γ_0 is an empirical resuspension parameter, and s_i is the normalised excess skin shear stress for class i:

$$s_i = \frac{\tau'_b - \tau'_{cri}}{\tau'_{cri}}. \tag{21}$$

The shear stresses τ'_b and τ'_{cri} in the above relationship are the spatially averaged skin shear stress over the ripple wavelength and its critical value for initiating sediment motion, respectively. The skin shear stress τ'_b is related to the shear stress spatially averaged over one ripple wavelength τ_b and the ripple height η according to the empirical relationship of Li (1994):

$$\tau'_b = |\vec{\tau}_b| \left[\delta \left(\frac{\sqrt{|\vec{\tau}_b|/\rho}}{\eta} \right) + \varphi \right]^2, \tag{22}$$

with $(\delta, \varphi) = (0.125 \text{ s}, 0.373)$ for $\sqrt{|\vec{\tau}_b|/\rho}\,/\eta < 2.3 \text{ s}^{-1}$, and $(\delta, \varphi) = (0.107\text{s}, 0.266)$ for $\sqrt{|\vec{\tau}_b|/\rho}\,/\eta \geq 2.3 \text{ s}^{-1}$.

Finally, the critical skin shear stress τ'_{cri} is determined from the schematised formula after Miller et al. (1977), modified from that proposed by Yalin (1972).

The low-concentration approximation of the entrainment rate expressed by Eqs. (19) and (20) is very similar to the Nielson's formula used by Beach and Sternberg (1988, 1992).

In the absence of wind, the shear stress, the turbulent kinetic energy k and the dissipation rate of the turbulent kinetic energy ε are assumed to have zero vertical gradients at the free surface, thus:

$$\frac{\partial\langle u\rangle}{\partial z}=0,\quad \frac{\partial\langle v\rangle}{\partial z}=0, \tag{23}$$

$$\frac{\partial k}{\partial z}=0, \tag{24}$$

$$\frac{\partial \varepsilon}{\partial z}=0. \tag{25}$$

Celik and Rodi (1984b) proposed a Dirichlet surface boundary condition for ε to take into account eddy damping near the free surface. Although this has not been tried in the present model, we suspect this would have little influence on the results given that the main focus of the paper here is on the near-bed layer.

The free surface boundary condition for the suspended sediment concentration $\langle c_i\rangle$ is:

$$w_{si}\langle c_i\rangle+\gamma_{\mathrm{t}}\frac{\partial\langle c_i\rangle}{\partial z}=0. \tag{26}$$

3. Numerical solution

A finite difference approach is adopted to solve the set of governing partial differential equations Eqs. (1)–(3), (11) and (12).

A staggered computational grid is used. The turbulent quantities ($\langle u'w'\rangle$, $\langle v'w'\rangle$, $\langle c'_iw'\rangle$, υ_t, γ_t, k, ε) are computed at the cell centres, whereas the mean variables ($\langle u\rangle$, $\langle v\rangle$, $\langle c_i\rangle$) are computed at the cell boundaries. A fine constant computational grid spacing is adopted in the layer adjacent to the bottom due to the rapid variation of the variables. Above this inner computational layer and to a given elevation (intermediate computational layer), the grid spacing increases linearly with the distance from the seabed to a value kept constant up to the free surface (outer computational layer). The thickness of the inner computational layer is taken as 0.3 m. The grid spacing in this layer is 5×10^{-4} m. The grid spacing in the outer computational layer ($z>3$ m) is 0.1 m.

The finite difference approximations are forward-differenced in time. The time step is taken equal to $T/720$, where T is the tidal period. The $k-\varepsilon$ Eqs. (11) and (12) are linearised with respect to the variable solved for in each equation. The production term in the equation for k is treated explicitly. Spatial derivatives are approximated by central differences, except for the advective term in the equation for $\langle c_i\rangle$ (Eq. (3)), which is upwind-differenced. This avoids oscillations in the solution when vertical convection dominates diffusion in Eq. (3). Such oscillations occur especially around slack waters when a central difference formula is used. Relaxation of k and ε at the end of each time step was found necessary to achieve stability. The relaxation scheme for quantities $Q = k$ and ε is $Q^{(n+1)} = (1-\theta)Q^{(n)} + \theta Q^{(n+1/2)}$ with $Q^{(n)}$ the variable at the old time step, $Q^{(n+1/2)}$ the new variable prior to relaxation, and $Q^{(n+1)}$ the final updated value at the new time step. A value $\theta = 0.9$ of the relaxation coefficient was found efficient in most situations. The stability of the solution is improved by increasing the diagonal dominance in the equation for k; hence the dissipation term in the right-hand side of Eq. (11) is weighted with the ratio of k at the new time step, divided by k at the old time step.

The resulting finite difference equations are of the tridiagonal type. They are solved with Thomas' algorithm at each time step.

4. Field measurements

4.1. Measurement area

The measurements used here were obtained at two shallow sites located in the eastern part of the English Channel (Fig. 1). The first measuring point is situated 1 nautical mile off Hardelot beach at latitude 50°38.00′N and longitude 1°33.32′E in mean water depth of 16.5 m. The second measuring point is located 2.5 nautical miles off Merlimont beach at latitude 50°27.00′N and longitude 1°32.20′E in mean water depth of 13.5 m. Echo sounder surveys showed the bottom in these areas to be featureless and flat. The tidal period was semi-diurnal ($T = 12.4$ h) with a spring tide range of approximately 7 m. The bottom sediment at the Hardelot site is a silty sand with a median grain size of 225 μm comprising 11% silt and very fine sand, 48% fine sand, 28% medium sand, 5% coarse sand and 8% very coarse sand (Fig. 2). The bed material at the Merlimont site is sand with a medium grain size of 256 μm comprising 7% silt and very fine sand, 39% fine sand, 50% medium sand, 4% coarse and very coarse sand.

4.2. Instrumentation

The instrumentation was deployed from the R/V Côtes de la Manche at the Hardelot site over the period 21–24 September 1997 and at the Merlimont site over the period 25–28 September 1997. Fair weather conditions prevailed during the experiment. The instrumentation system is a heavily weighted benthic tripod, called SAMBA (Station d'Acquisition de Mesure Benthique Autonome), equipped with two self-recording instruments: (i) an Integrated Instrument Programmable Package (I2P2) resolving the inner bottom boundary layer, and (ii) an upward-looking 1200 kHz Broad-Band Acoustic Doppler Current Profiler (BBADCP) scanning the outer bottom boundary layer.

The I2P2 incorporates a Paroscientific pressure sensor located at $z = 2.17$ m above the bottom and a vertical array of four Marsh–McBirney 3.8-cm diameter electromagnetic current meters measuring the horizontal velocities at heights $z = 0.3$, 0.6, 0.9 and 1.4 m above the seabed. Its data logger was programmed to sample every half-hour at a

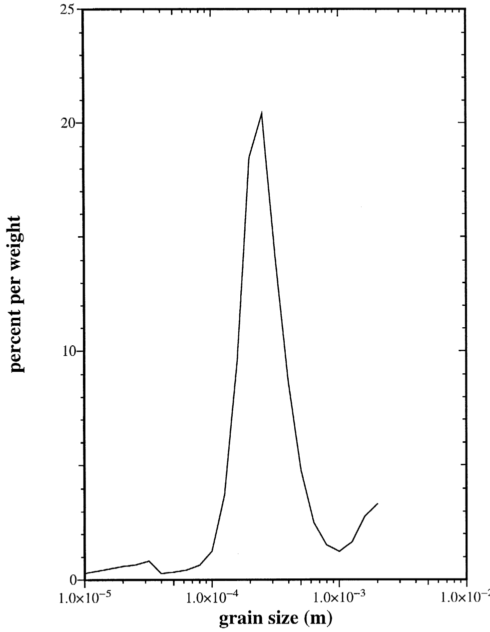

Fig. 2. Grain size frequency distribution of seabed sediments at the Hardelot site.

rate of 4 Hz in 9-min records (in logger parlance ‘bursts’, referred to later). The BBADCP measured 5 min-averaged horizontal currents and acoustic backscatter strength profiles. Its spatial resolution was 1 m in the vertical direction and the sampling rate was 5 min. The lowermost measuring point was 5 m above the seabed.

4.3. Data reduction procedures

4.3.1. I2P2 data

Considering the objective of estimating the turbulent kinetic energy k within the inner boundary layer, the linear trend of the horizontal velocity components was first removed from the raw data u and v. This yields the time series of the velocity fluctuations $u' = u - \langle u \rangle$ and $v' = v - \langle v \rangle$.

In spite of calm weather conditions, surface gravity waves generated by a light northeasterly breeze were present during the experiment. The velocity field induced by the surface waves is contained in the velocity fluctuations u' and v', and this is likely to alter the estimate of the turbulent kinetic energy throughout the water column. The pressure data were used to remove the orbital contributions to u' and v'. The raw pressure data p are made up of two contributions, namely,

$$p = \langle p \rangle + \tilde{p}, \tag{27}$$

where $\langle p \rangle$ is the linear trend representing the sum of the tidal modulation and the mean atmospheric pressure, and $\tilde{p}$ the oscillating pressure induced by the surface waves. The turbulent pressure fluctuation p' is neglected, which is in agreement with the absence of wave breaking in the present field data. Removing the mean atmospheric pressure measured at Boulogne-sur-Mer and applying the hydrostatic approximation convert $\langle p \rangle$ to water depth $\langle h \rangle$ at the measuring point. Time series of the wave elevation ξ is obtained with linear wave theory using the time series of the oscillating pressure $\tilde{p}$. This is done in the Fourier space for each individual spectral ray satisfying the dispersion equation of linear water waves. The significant wave heights and averaged wave periods are then computed from a wave-by-wave analysis of ξ time series. For each burst, the horizontal and vertical root-mean-squared orbital velocities $\tilde{U}_z$ and $\tilde{w}_z$ at elevation z above the seabed are obtained from linear wave theory. These are used to estimate the averaged turbulent kinetic energy k at the same elevation z according to:

$$k = \frac{\alpha}{2}\left(\langle u^{2\prime} \rangle + \langle v^{2\prime} \rangle\right) - \frac{1}{2}\left(\tilde{U}_z^2 + \tilde{w}_z^2\right), \tag{28}$$

where α is a factor compensating for the missing third velocity component; $\alpha = 1.4$ is relevant for oscillatory boundary layers (Justesen, 1988; Thais et al., 1999).

In practice, we have here $\tilde{w}_z \ll \tilde{U}_z$ since the I2P2 measured very near to the seabed. In the present field experiment, the dominant wave was 4 s in period. A cross-spectral analysis between ξ, u' and v' showed that the dominant wave was travelling southwest. The significant wave height H_S never exceeded 0.4 m, averaging 0.2 m. This corresponds to a 'background' orbital velocity at the bottom of 3 cm s^{-1}. This value produces an orbital kinetic energy around 10% of the peak turbulent kinetic energy over the 6 days of measurements (see Section 5).

Such wave velocities are small compared to the tidal current, except maybe at times of flow reversal. Little wave–current interactions near the bottom are therefore to be expected. Also, it is unlikely that wave mixing modified significantly the structure of the flow in the water column. The present data set appears as a good candidate for testing a model of a tidally driven bottom boundary layer.

4.4. BBADCP data

Only the acoustic backscatter strength recorded by the BBADCP at the Hardelot site was of good quality and will be considered here. The raw data were calibrated to yield estimates of suspended particulate matter concentration, consisting primarily of sediment. The calibration exercise was based on a series of water samples collected over two tidal cycles within the water volume ensonified by the BBADCP ($z = 5$ and 8 m). Details of the field calibration are given in Chapalain et al. (1999).

5. Application

5.1. Model set-up

The oscillating sea surface slope that provides the tidal forcing of the one-dimensional model is derived from a two-dimensional vertically integrated shallow-water model which covers the eastern part of the English Channel and the southern part of the North Sea (Fig. 1B). The finite-difference model used is the MECCA model developed by Hess (1986). Details about this model can be found in Hess (1986). The horizontal resolution is 1×1 km^2. The model is driven by imposing the tidal elevations produced by the 30 major harmonic constituents along the open boundaries of the computational domain. The simulation is initiated 13 tidal cycles before the beginning of the field measurements at the first site. The end of the spin-up is characterised by equinoctial tidal conditions.

5.2. Results and discussion

Figs. 3–6 show the model predictions for the west–east ($\langle u \rangle$) and south–north ($\langle v \rangle$) velocity components 0.6 and 5 m from the seabed together with the measurements at the two experimental sites. The origins of the time series at the Hardelot site (Figs. 3 and 4) and the Merlimont site (Figs. 5 and 6) correspond to 14:15 21 September 1997 and 17:55 25 September 1997, respectively. The south–north component dominates the current predominantly flowing north and ebbing south almost parallel to the coastline. One sees a reasonably good agreement between measurements and predictions of the south–north component at the two sites, both in phase and amplitude. The asymmetry with respect to the vertical axis is clearly seen for the $\langle v \rangle$ velocity component: the current variation around slack water is faster before the flood current than before the ebb current. This is fairly well reproduced by the model. The measured southward current is marginally smaller than predicted by the model at the Merlimont site in the outer boundary layer (Fig. 6). The predicted vertical variation in the maximum south–north current component between 0.6 and 5 m above the seabed is acceptable.

Conversely, the model overpredicts the west–east current amplitude at the Hardelot site (Figs. 3 and 4). The difference between predicted and measured values at $z = 0.6$ m is maximum during the first two tidal cycles characterised by spring tide conditions (Fig. 3). Later in the time series, this difference tends to decrease, but remains significant. We speculate that the discrepancy is the consequence of neglecting the advective terms in the momentum equations of the one-dimensional model. The Hardelot measuring point being located very near the coastline, these advective terms may have a non-negligible influence on the west–east velocity component which is at a right angle with the coastline. Results from the two-dimensional vertically integrated MECCA model, which includes the advective terms, are indeed better at elevation $z = 5$ m corresponding roughly to the height where the velocity of an idealised logarithmic flow is equal to its vertically averaged value. This conviction also rests upon the following argument: predictions at the Merlimont site 1.5 nautical miles farther from the coastline than the Hardelot site are indeed better in spite of a slight phase advance in the model-predicted west–east velocity component (Figs. 5 and 6).

Model predictions of the turbulent kinetic energy at $z = 0.3$, 0.6, 0.9 and 1.4 m above the seabed are plotted with the measured time series at the Hardelot and Merlimont sites in Figs. 7 and 8. The vertically uniform structure of the turbulent kinetic energy consistent with a constant stress layer is reproduced by the model. The phase of the tidal modulated signal is well simulated by the model at both locations. A close inspection of

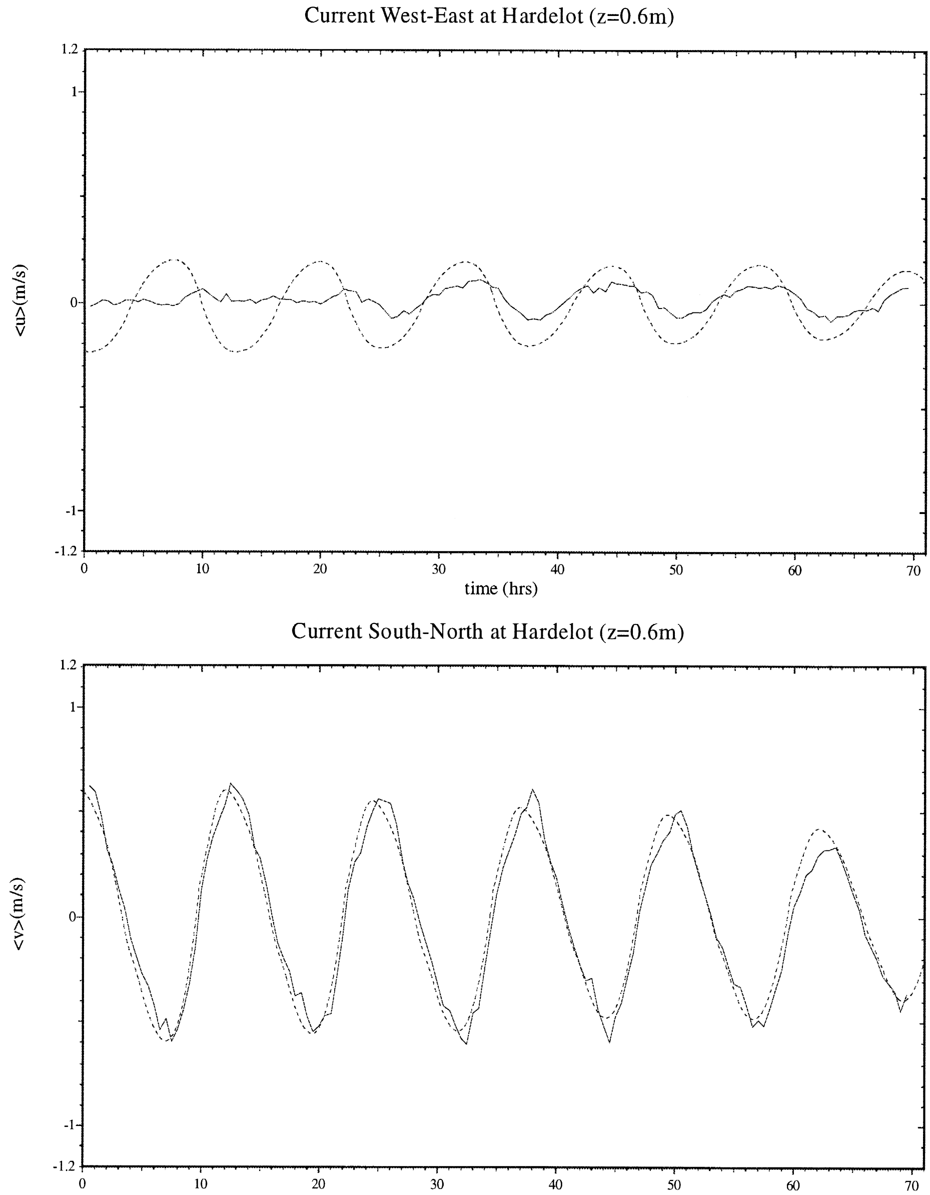

Fig. 3. Time series of measured (solid line) and model-predicted (dashed line) west–east and south–north velocity components at $z = 0.6$ m above the seabed at the Hardelot site.

the results reveals that the computed turbulent kinetic energy peaks suffer some discrepancies. At the Hardelot site, the predictions are seen to significantly overestimate the field measurements during the first part of the time series. There is a particular spell of 12 h ($16 \text{ h} < t < 28 \text{ h}$) where the model fails by more than a 100% in the prediction

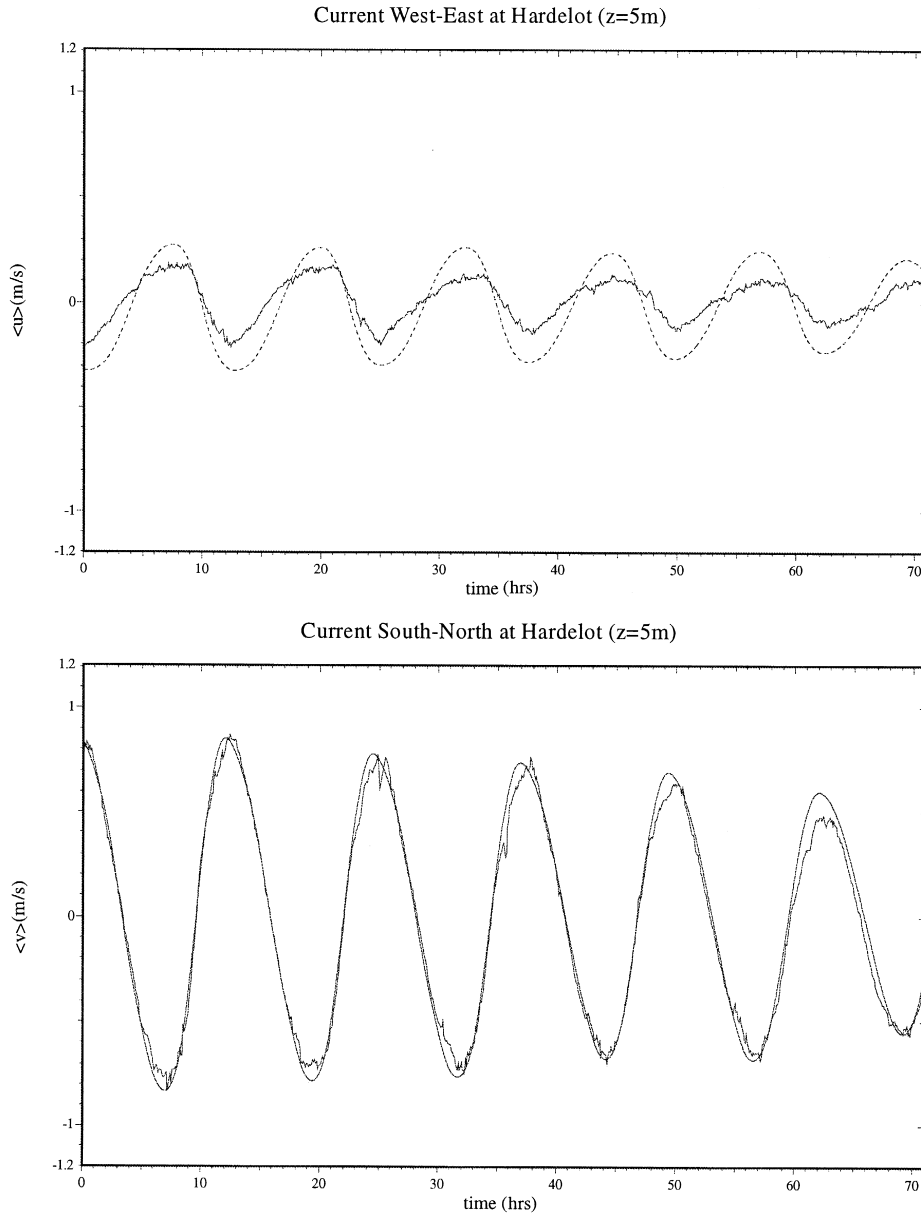

Fig. 4. Time series of measured (solid line) and model-predicted (dashed line) west–east and south–north velocity components at $z = 5$ m above the seabed at the Hardelot site.

of the peaks. At this stage, we can only remark that this failure is coincident with the poor prediction of the west–east velocity component seen in Fig. 3, i.e. at $z = 0.6$ m. We should stress, on the other hand, that the model predictions appear much better during the second part of the time series. A good agreement between model predictions

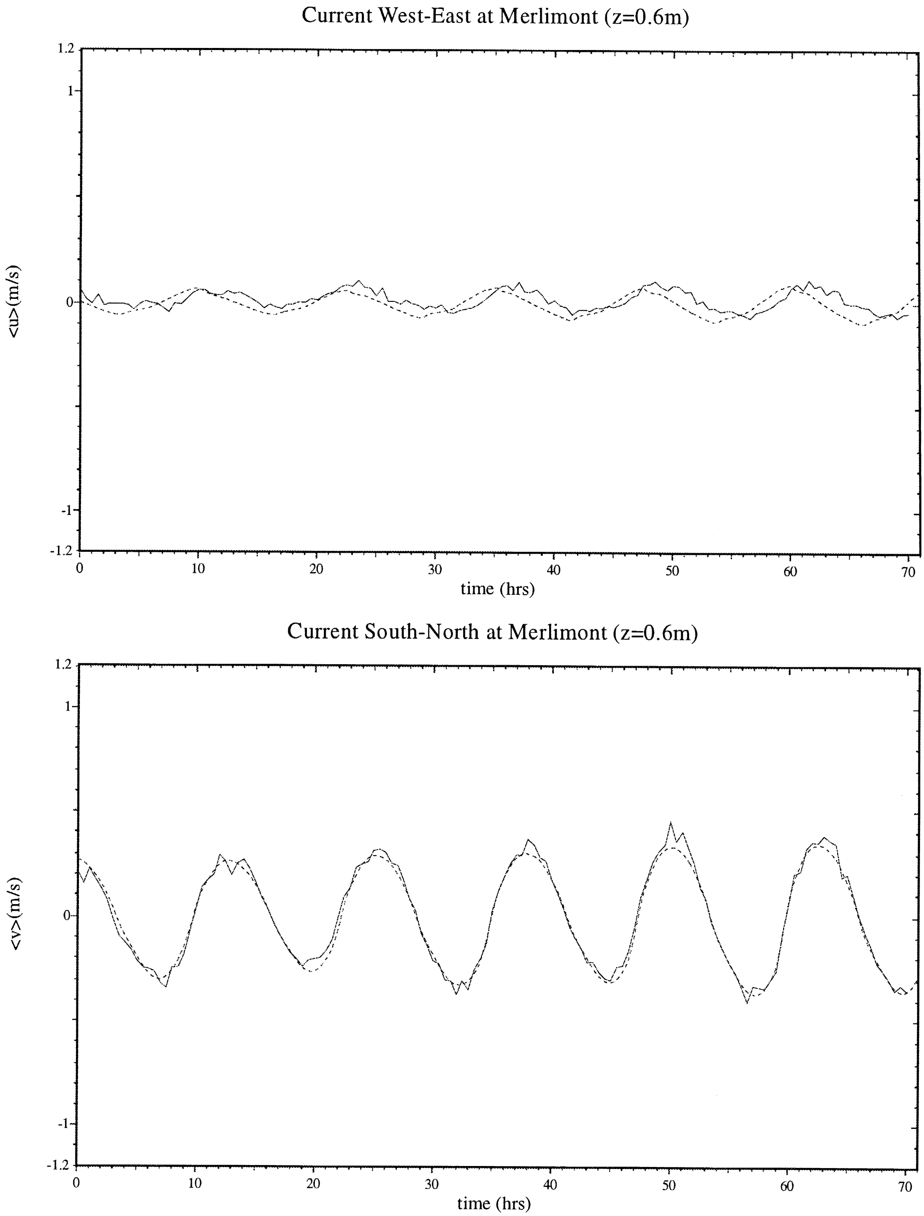

Fig. 5. Time series of measured (solid line) and model-predicted (dashed line) west–east and south–north velocity components at $z = 0.5$ m above the seabed at the Merlimont site.

and experimental data is noticed at the Merlimont site. We just notice a small underprediction of the turbulence level during the last four flood current peaks.

In spite of errors in the prediction of the west–east velocity component at the Hardelot site, it should be pointed out that the errors remain small when scaled with the

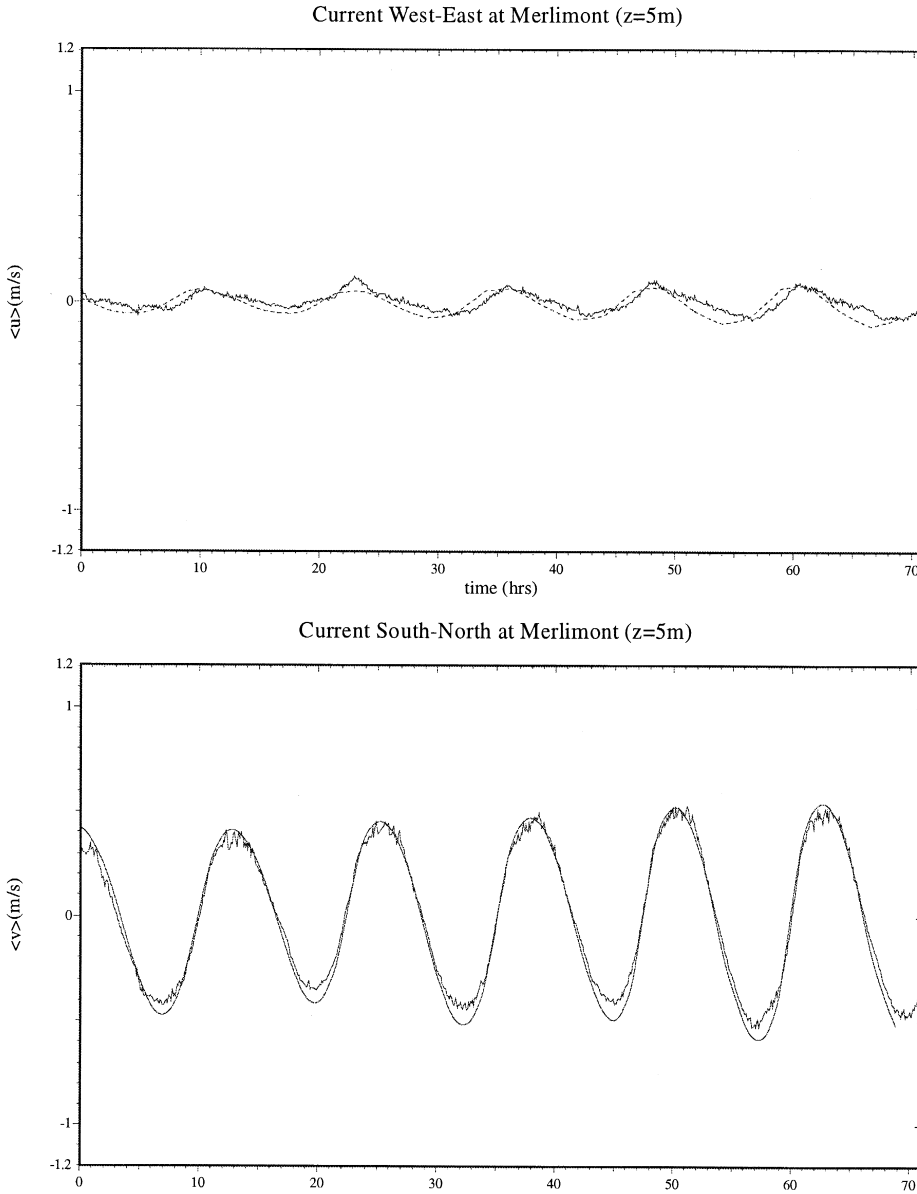

Fig. 6. Time series of measured (solid line) and model-predicted (dashed line) west–east and south–north velocity components at $z = 5$ m above the seabed at the Merlimont site.

horizontal velocity amplitude (of order 5–10%) and should have moderate consequences on the prediction of the suspended sediment concentration. The computations were performed for an available assemblage of 18 different classes of sediment reproducing distributions of natural sediment. The finest class taken into account is 45 μm. The

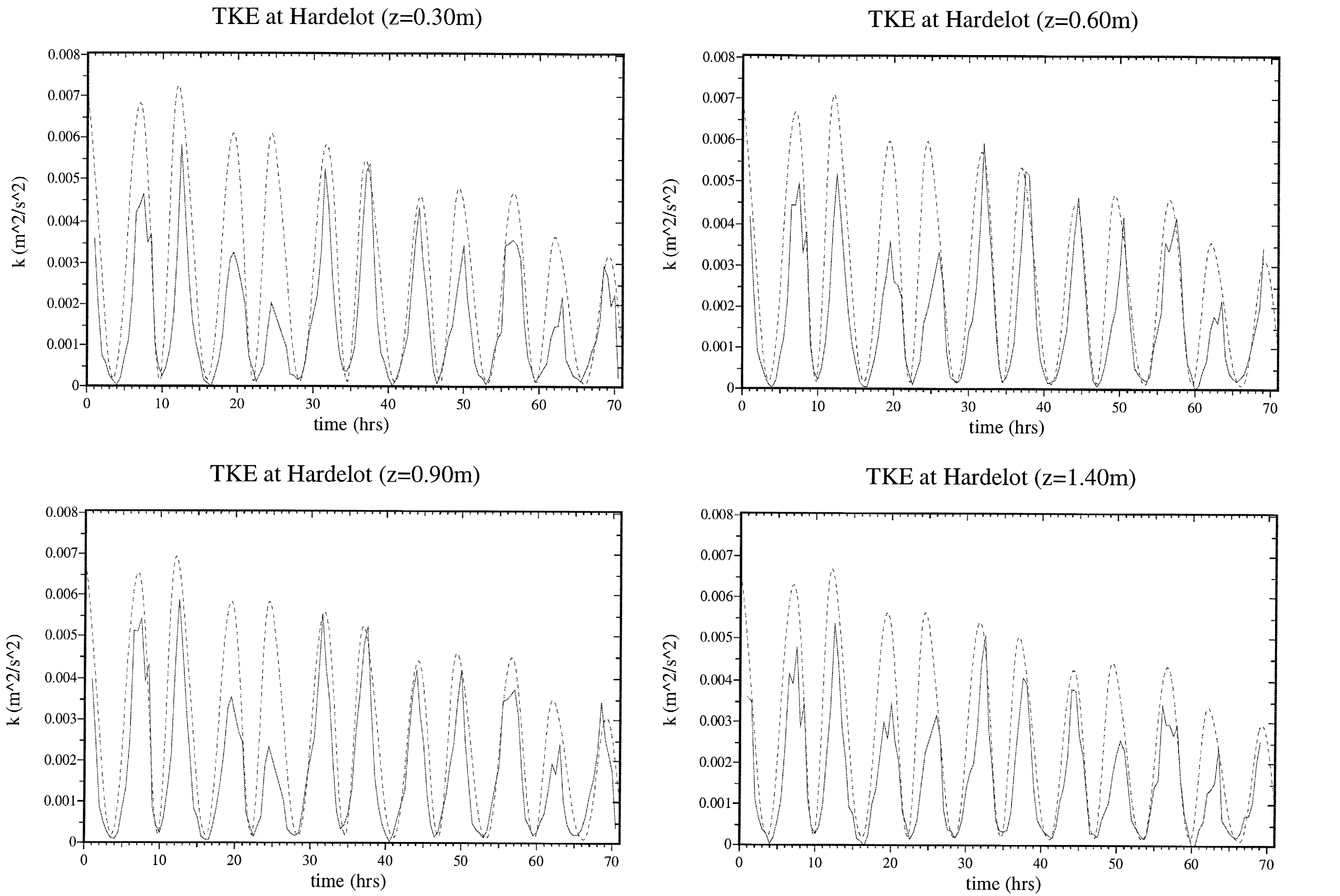

Fig. 7. Time series of measured (solid line) and model-predicted (dashed line) turbulent kinetic energy at $z = 0.3$, 0.6, 0.9 and 1.4 m above the seabed at the Hardelot site.

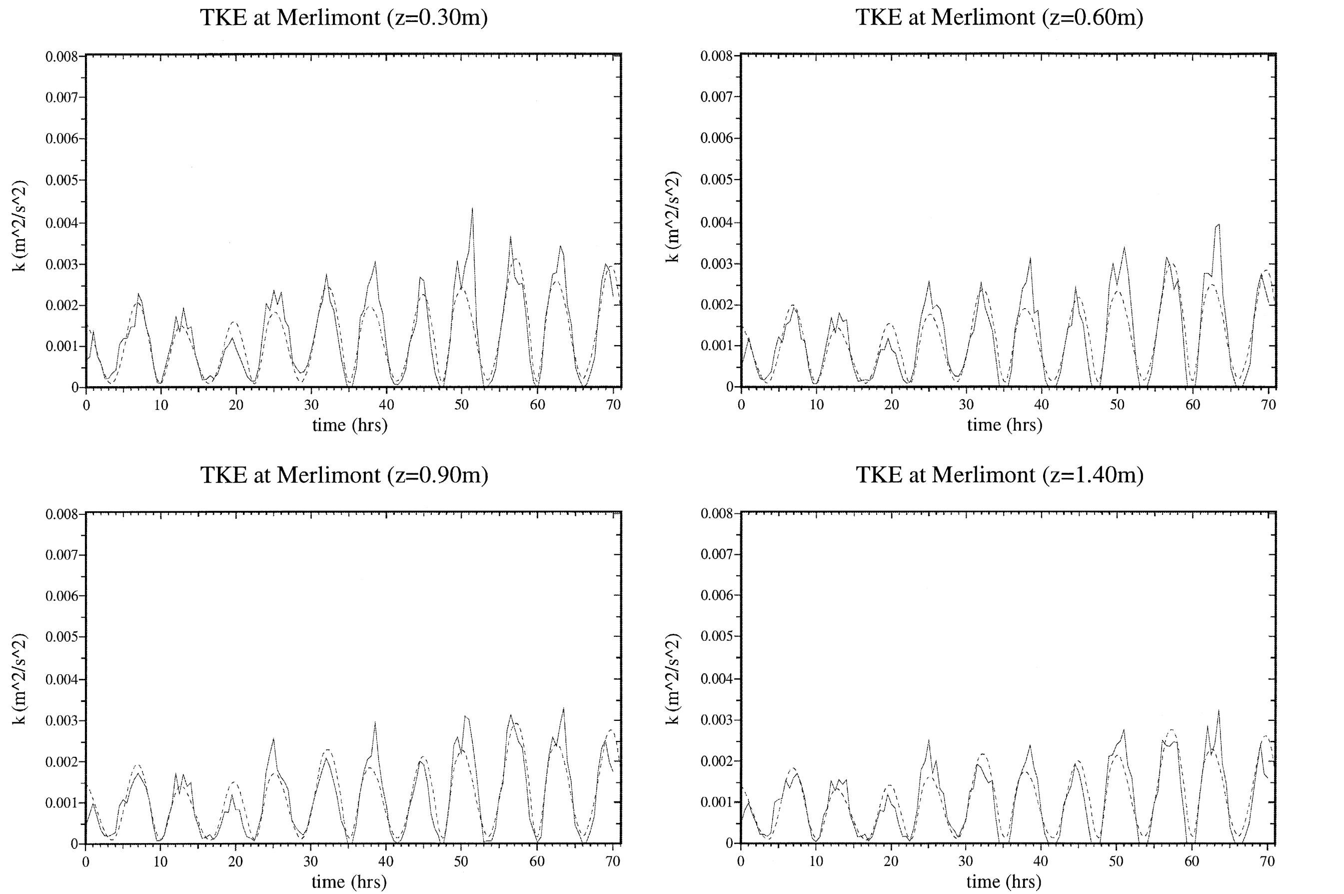

Fig. 8. Time series of measured (solid line) and model-predicted (dashed line) turbulent kinetic energy at $z = 0.3$, 0.6, 0.9 and 1.4 m above the seabed at the Merlimont site.

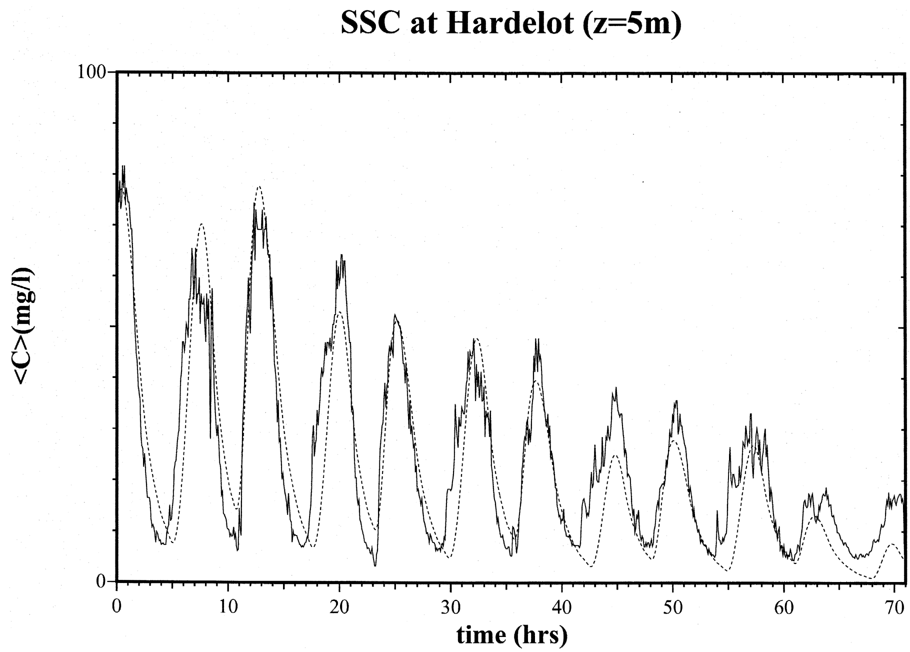

Fig. 9. Time series of measured (solid line) and model-predicted (dashed line) total suspended sediment concentration at $z = 5$ m above the seabed at the Hardelot site.

model is run by adjusting the value of the resuspension parameter γ_0 in Eq. 20 until predicted and measured total suspended sediment concentrations ($\langle C \rangle$) at 5 m above the seabed are in reasonable agreement (Fig. 9). The adjustment is focused on the second part of the time series ($t > 28$ h) when the bottom boundary layer turbulence is better simulated by the model. A best fit value of $\gamma_0 = 6.5 \times 10^{-3}$ was found. This value is two to three times larger than those recommended by Smith and McLean (1977) and Glenn and Grant (1983) on the basis of observations in rivers and flumes, and is one to two orders of magnitude larger than the values which Dyer (1980), Wiberg and Smith (1983), Drake and Cacchione (1989) and Vincent and Green (1990) obtained from continental shelf data. The general pattern of the total suspended sediment concentration, which is the result of alternate resuspension and deposition of bottom sediments by tidal scour, is satisfactorily predicted by the model. The model reproduces the phase and magnitude of the successive peaks influenced by the tidal currents asymmetry. It is also found to simulate fairly well the variation of sediment resuspension processes associated with the neap–spring cycle.

6. Conclusions

We have presented a model of a tidal boundary layer with suspended sediments. Key features of the flow are the simultaneous interactions between the oscillatory and turbulent flow; suspended sediments; sediment entrainment; and fallout. The model rests upon the assumption of an idealised one-dimensional flow with sediment treated as a continuum. The flow is driven by an oscillatory horizontal pressure gradient derived from a two-dimensional vertically integrated tidal model. The model solves the momentum and suspended sediment concentration equations with an algorithm for exchanges of mass at the water–sediment interface. A standard $k-\varepsilon$ turbulence closure scheme is employed to determine the Reynolds shear stresses and the vertical eddy fluxes of suspended sediment. Standard empirical constants were used in the turbulence model. Ripple effects on the boundary layer structure and the partitioning of skin friction from form drag were included.

The model was applied to the eastern part of the English Channel. The model predictions were compared with field measurements collected at two sites by the instrumented benthic tripod, SAMBA. Moderate agreement was found at the Hardelot site, whereas good agreement was observed at the Merlimont site regarding all the major features of the tidal flow. Particularly, the model tends to overestimate the currents and the turbulent kinetic energy at the Hardelot site situated very close to the coastline. We insist that no parameter tuning was applied on the hydrodynamics of the model. On the other hand, the sediment response to tidal forcing at the Hardelot site was satisfactorily predicted with a resuspension parameter $\gamma_0 = 6.5 \times 10^{-3}$.

To summarise, our model predictions appear to be physically sound. They are encouraging because they demonstrate that a one-dimensional model based on a fairly simple fluid dynamics approach may be used to calculate the time-dependent hydrodynamic and suspended sediment concentration fields in a tidally driven flow. In that respect, it is quite satisfactory that a one-dimensional model forced with pressure gradients computed with a two-dimensional (vertically integrated) model gives reasonable predictions at a much cheaper computational cost than fully three-dimensional coastal dynamics models. However, based on our field experiments, we should add that such an approach seems to bear limitations in areas very near to the coastline. The present results also illustrate that such a model, integrating various theories and parameterisations including the complex interrelationships between currents and movable sediments, is an efficient predictive tool useful for advancing our understanding of flow and sediment transport processes in tide-dominated environments.

Acknowledgements

This work was undertaken as part of the MAST III programme ‘PRe-Operational Modelling In the Seas of Europe’ (PROMISE) funded by the Commission of the European Union Directorate General for Science, Research and Development under contract no. MAS3-CT950025 and the research programme ‘DYnamique du Système COtier du Pas-de-Calais’ (DYSCOP) supported by the Nord-Pas de Calais Regional Council, the European programme FEDER, the Centre National de la Recherche Scientifique (CNRS) and the French Ministry of Universities and Research under contracts nos. DYSCOP-USTL-999/2486/9304, 999/2641/9384, and 999/2641/9385. The contribution made by H. Smaoui in the numerical resolution in the equation for ε and the application of the MECCA model to the eastern English Channel is gratefully acknowledged. We are indebted to the Service Hydrographique et Océanographique de la Marine (SHOM) for providing the harmonic components used to force the MECCA model. We express our acknowledgements to the Institut National des Sciences de l'Univers (INSU-CNRS) for supplying ship facilities (R/V Côtes de la Manche). Finally, we wish to thank the captain and the crew of the R/V Côtes de la Manche for their excellent work during the ESPRIS cruise.

References

ASCE Task Committee on Turbulence Models in Hydraulic Computations, 1988a. Turbulence modeling of surface water flow and transport: Part I. J. Hydraul. Eng. 114 (9), 970–991.

ASCE Task Committee on Turbulence Models in Hydraulic Computations, 1988b. Turbulence modeling of surface water flow and transport: Part II. J. Hydraul. Eng. 114 (9), 992–1014.

Augris, C., Clabaut, P., Dewez, S., Auffret, J.P., 1987. Surficial sediments map off Boulogne sur Mer (France) (1/43 600). Publication conjointe IFREMER et Région Nord-Pas de Calais.

Barenblatt, G.T., 1953. Motion of suspended particles in a turbulent flow. Prikl. Mat. Mekh. 17 (3), 261–274.

Baumert, H., Chapalain, G., Smaoui, H., McManus, J.P., Yagi, H., Regener, M., Sündermann, J., Szilagy, B., 2000. Modelling and numerical simulation of turbulence, waves and suspended sediments for pre-operational use in coastal seas. This volume.

Beach, R.A., Sternberg, R.W., 1988. Suspended sediment transport in the surf zone: response to cross-shore infragravity motion. Mar. Geol. 80, 671–679.

Beach, R.A., Sternberg, R.W., 1992. Suspended sediment transport in the surf zone: response to incident wave and longshore current interaction. Mar. Geol. 108, 275–294.

Boussinesq, J., 1877. Mémoire présenté par divers savants à l'Académie des Sciences de Paris. pp. 23–46.

Celik, I., Rodi, W., 1984a. A deposition entrainment model for suspended sediment transport. Report SFB 210/T/6, University of Karlsruhe, Karlsruhe, Federal Republic of Germany, 31 pp.

Celik, I., Rodi, W., 1984b. Simulation of free-surface effects in turbulent channel flows. Phys.-Chem. Hydrodyn. 5 (3/4), 217–227.

Celik, I., Rodi, W., 1985. Mathematical modelling of suspended sediment transport in open channels. Proceedings of the 21st Congress of the I.A.H.R. pp. 534–538.

Celik, I., Rodi, W., 1988. Modeling suspended sediment transport in non-equilibrium situations. Proc. ASCE, J. Hydraul. Eng. 114 (10), 1157–1191.

Celik, I., Rodi, W., 1991. Suspended sediment transport capacity for open channel flow. Proc. ASCE, J. Hydraul. Eng. 117 (2), 191–204.

Chapalain, G., Thais, L., 2000. An intercomparison of different turbulence closure schemes for tidal bottom boundary layer. In preparation.

Chapalain, G., Thais, L., Smaoui, H., 1999. Modeling of a tidal bottom boundary layer with suspended sediment. Hydrobiologia 414, 1–12.

Davies, A.M., Luyten, P.J., Deleersnijder, E., 1995. Turbulence energy models in shallow sea oceanography. Quantitative Skill Assessment for Coastal Ocean Models, Coastal and Estuarine Studies. AGU 47, pp. 97–123.

Drake, D.E., Cacchione, D.A., 1989. Estimates of the suspended sediment reference concentration (C_a) and resuspension coefficient (γ_0) from near-bed observations on the California shelf. Cont. Shelf Res. 9, 51–64.

Dyer, K.R., 1980. Current velocity profiles over rippled bed and the threshold of movement of sand. Estuarine Coastal Mar. Sci. 10, 181–189.

Gibbs, R.J., Matthew, M.D., Link, D.A., 1971. The relation between sphere size and settling velocity. J. Sediment. Petrol. 41, 7–18.

Glenn, S.M., Grant, W.D., 1983. Continental shelf bottom boundary layer model. Theoretical model development. Vol. 1. Technical report to Pipeline Research Committee American Gas Association, Arlington, VA, 164 pp.

Hess, K.W., 1986. Numerical model of circulation in Chesapeake Bay and the continental shelf. NOAA Technical Memorandum NESDIS AISC. 6, National Environmental Satellite, Data, and Information Service, NOAA, U.S. Department of Commerce, 47 pp.

Justesen, P., 1988. Prediction of turbulent oscillatory flow over rough beds. Coastal Eng. 12, 257–284.

Lavelle, J.W., Mofjeld, H.O., Baker, E.T., 1984. An in situ erosion rate for a fine-grained marine sediment. J. Geophys. Res. 89 (C4), 6543–6552.

Li, M.Z., 1994. Direct skin friction measurements and stress partitioning over movable sand ripples. J. Geophys. Res. 99 (C1), 791–799.

Lick, W., 1982. Entrainment, deposition, and transport of fine-grained sediments in lakes. Hydrobiologia 91, 31–40.

Lumley, J.L., 1978. Two-phase and non-Newtonian flows. In: Bradshaw, P. (Ed.), Topics in Applied Physics 12 Springer-Verlag, New York, pp. 289–324.

Miller, M.C., McCave, I.N., Komar, P.D., 1977. Threshold of sediment motion under unidirectional currents. Sedimentology 24, 507–527.

Rodi, W., 1980. Turbulence models and their application in hydraulics, Book Publication of the International Association of Hydraulic Research, Delft, The Netherlands. 104 pp.

Rodi, W., 1981. Examples of turbulence models for incompressible flows. AIAA J. 20 (7), 872–879.

Rodi, W., 1987. Examples of calculation methods for flow and mixing in stratified fluids. J. Geophys. Res. 92 (C5), 5305–5328.

Smith, J.D., McLean, S.R., 1977. Spatially averaged flow over a wavy surface. J. Phys. Oceanogr. 82 (12), 1735–1746.

Soo, S.L., 1967. Fluid Dynamics of Multiphase Systems. Blaisdell Publishing, Waltham, MA, 524 pp.

Soulsby, R.L., Wainwright, B.L.S.A., 1987. A criterion for the effect of suspended sediment on near-bottom velocity profiles. J. Hydraul. Res. 25 (3), 341–355.

Thais, L., Chapalain, G., Smaoui, H., 1999. Reynolds number variation in oscillatory boundary layers: Part I. Purely oscillatory motion. Coastal Eng. 36 (2), 111–146.

van Rijn, L.C., 1986. Mathematical modeling of suspended sediment in non-uniform flows. Proc. ASCE, J. Hydraul. Eng. 112 (6), 1613–1641.

Vincent, C.E., Green, M.O., 1990. Field measurements of the suspended sand concentration profiles and fluxes, and of the resuspension coefficient γ_0 over a rippled bed. J. Geophys. Res. 95, 15591–15601.

Wiberg, P.L., Smith, J.D., 1983. A comparison of field data and theoretical models for wave–current interactions at the bed on the continental shelf. Cont. Shelf Res. 2, 147–162.

Wooding, R.A., Bradley, E.F., Marshall, J.K., 1973. Drag due to regular arrays of roughness elements of varying geometry. Boundary Layer Meteorol. 5, 285–308.

Yalin, M.S., 1972. Mechanics of Sediment Transport. Pergamon, New York, 290 pp.

Yalin, M.S., 1985. On the determination of ripple geometry. Proc. ASCE, J. Hydraul. Div. 111 (8), 1148–1155.